

Dilepton flow and deconfinement phase transition in heavy ion collisions

Jian Deng,^{1,2} Qun Wang,¹ Nu Xu,³ and Pengfei Zhuang⁴

¹*Interdisciplinary Center for Theoretical Study and Department of Modern Physics, University of Science and Technology of China, Anhui 230026, People's Republic of China*

²*School of Physics, Shandong University, Jinan, Shandong 250100, China*

³*Nuclear Science Division, Lawrence Berkeley National Laboratory, Berkeley, California 94720, USA*

⁴*Physics Department, Tsinghua University, Beijing 100084, China*

The dilepton radial flow in Au+Au collisions at $\sqrt{s_{NN}}=200$ GeV is investigated. The space-time evolution of the fireball is described by a 2+1 dimensional ideal hydrodynamics with a variety of equations of state. The slope parameters of the transverse momentum spectra from the partonic and hadronic phases show distinct features and are sensitive to equation of state parameters. The elliptic flow and breaking of M_T scaling are also studied and have distinct features for the two phases. These features can serve as clean signals for the formation of a quark-gluon plasma in ultra-relativistic heavy ion collisions.

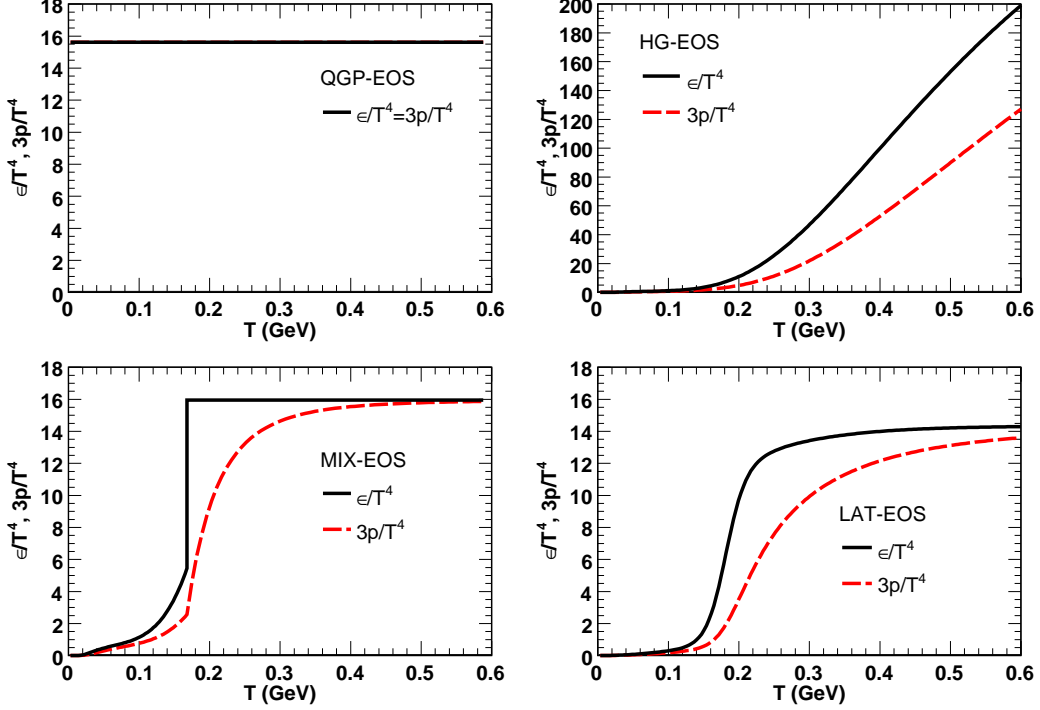
I. INTRODUCTION

Among all observables for determining the quark gluon plasma (QGP) in heavy ion collisions, the electromagnetic probes such as photons and dileptons are expected to provide clean signatures due to their instant emissions once produced [1–11]. These thermal photons and dileptons contain undistorted information about the space-time trace of the new state of matter formed in such collisions. There are many sources of dileptons in heavy ion collisions. In the lower invariant mass region ($M \lesssim 1$ GeV) dileptons are mainly from resonance decays and may be related to chiral symmetry restoration [12–15]. In the higher invariant mass region ($M \gtrsim 3$ GeV) dileptons are dominated by the Drell-Yan process and charmonium decays. For moderate invariant mass dileptons ($1 \lesssim M \lesssim 3$ GeV), it was argued that dileptons from semileptonic decays of correlated open charm in pp collisions are dominant [16]. But in Au+Au collisions, both charm related single lepton contributions and their dynamic correlations are expected to be suppressed by medium modification. Therefore thermal radiation may play important role in the intermediate mass region and the dilepton spectra can be used to extract thermodynamic parameters of the fireball.

The observation of jet quenching and strong elliptic flow at the Relativistic Heavy Ion Collider (RHIC) at Brookhaven National Laboratory tell us that the dense matter produced at RHIC interacts strongly and may reach local thermalization in very short time [17, 18], implying that ideal hydrodynamic models are applicable to such systems [19, 20]. In contrast to hadronic flow, the observables of dileptons are more direct and penetrating probes to the early space-time profile of the QGP [9, 10]. The radial flow of thermal dileptons has been measured at CERN super-proton synchrotron (SPS) by the NA60 collaboration [21]. It was found that the inverse slope parameter T_{eff} increases with the invariant mass M of the lepton pair below the ρ meson mass and then starts decreasing above $M \sim 1$ [21]. The reason for the drop of T_{eff} around $M \sim 1$ GeV is not fully understood although it was thought to be an indication of the transition to an emission source with much smaller flow possibly a partonic source [21, 22]. The observed strong correlation of T_{eff} versus M in the region $M \lesssim 1$ GeV is mainly due to the collectivity developed in the hadronic stage at SPS energies. Should the collectivity have been developed in the partonic phase of the evolution in high energy nuclear collisions, RHIC and/or LHC, one would also expect to see the increase of T_{eff} in the intermediate mass region $1 \lesssim M \lesssim 3$ GeV. Inspired by the NA60 result and in order to develop clean observables for the formation of the QGP, we propose to study the transverse momentum distributions of di-electrons over the entire region of $0.5 \lesssim M \lesssim 3$ GeV.

In this paper we use a 2+1 dimensional ideal hydrodynamic model to give the space-time evolution of the medium created in Au+Au collisions at $\sqrt{s_{NN}}=200$ GeV. Our program gives results consistent with AZHYDRO [23]. To include the pre-equilibrium emission of the di-electrons at very beginning, we set the initial time for the hydrodynamic evolution $\tau_0 = 0.2$ fm/c as in Ref. [9] instead of $\tau_0 = 0.6$ fm/c in previous studies. The initial transverse energy density is calculated in the Glauber model with the peak temperature being at about 520 MeV in central collisions. Another critical input is the equations of state (EOS) of the dense matter [24]. We choose four types of EOS, (i) QGP-EOS, the ideal gas EOS for 3-flavor QGP, $\epsilon = 3p = (19/12)\pi^2 T^4$ without the hadronic phase; (ii) HG-EOS, the resonance hadron gas EOS for the hadron gas (HG) [25] without the partonic phase; (iii) MIX-EOS, the one with the first order phase transition with both the partonic and hadronic phases [25]; (iv) LAT-EOS, the one extracted from the lattice calculations [26]. Note that in the MIX-EOS and LAT-EOS there are partonic and hadronic components. These EOS are shown in Fig. 1. We put emphasis on the lattice EOS which can describe the crossover from resonance HG to QGP in the temperature range 180-200 MeV. Other EOS are also considered in our calculations for the purpose of comparison. Although the crossover does not have a rigorous critical temperature T_c to separate the QGP from

FIG. 1: Equations of state: QGP-EOS (upper-left), HG-EOS (upper-right), MIX-EOS (lower-left), LAT-EOS (lower-right).



the HG phase, we still choose $T_c = 180$ MeV as a tuning parameter. The freezeout temperature is set to $T_f = 120$ MeV below which there is no di-electron emission from the HG sector. The post-freezeout di-electron decay of the ρ mesons is not included directly in our calculation, whose effect on the di-electron spectra can be partly taken into account by lower the freezeout temperature. The fine tuning of T_c and T_f does not qualitatively change our results and conclusions.

II. DILEPTON YIELDS

In the thermalized medium HG or QGP, the rate for the di-lepton production per unit volume is given by [3–5],

$$\frac{d^4N}{d^4x d^4p} = -\frac{\alpha}{4\pi^4} \frac{1}{M^2} n_B(p \cdot u) \left(1 + \frac{2m_l^2}{M^2}\right) \sqrt{1 - \frac{4m_l^2}{M^2}} \text{Im}\Pi^R(p). \quad (1)$$

Here m_l is the lepton mass, $\alpha = e^2/(4\pi)$ is the fine structure constant with the electric charge e for leptons, $p = (p_0, \mathbf{p}) = p_1 + p_2$ is the dilepton 4-momentum and $M = \sqrt{p^2}$, $n_B(p \cdot u) = 1/(e^{p \cdot u/T} - 1)$ is the Bose distribution function with T and u the local temperature and medium velocity respectively, $\Pi_{\mu\nu}^R$ is the retarded photon polarization tensor from the quark-loop or the hadronic loop, and $\Pi^R = \frac{1}{3}\Pi_{\mu}^{R\mu}$. For the hadron gas, Π^R is further related to the retarded rho-meson propagator D_{ρ}^R via $\text{Im}\Pi^R = -(e^2 m_{\rho}^4 / g_{\rho}^2) \text{Im}D_{\rho}^R$, where g_{ρ} is the photon-rho-meson coupling constant in the vector meson dominance model, and m_{ρ} is the rho-meson mass. The imaginary part of the retarded ρ -meson propagator is given by,

$$\text{Im}D_{\rho}^R = \frac{\text{Im}\Pi_{\rho}^R}{(p^2 - m_{\rho}^2 + \text{Re}\Pi_{\rho}^R)^2 + (\text{Im}\Pi_{\rho}^R)^2}, \quad (2)$$

where Π_{ρ}^R is the retarded rho-meson polarization tensor contraction. We assume that the hadron gas is mainly composed of mesons and consider following mesonic vertices for the ρ meson [5] in Π_{ρ}^R : $\rho\pi X$ and $\rho K K'(1270)$, where X denotes meson resonances below 1300 MeV, namely, ω , $h_1(1170)$, $a_1(1260)$ and $\pi'(1300)$. Here we neglect the baryonic contributions since the collisional energy considered in this paper is the RHIC energy (200 GeV) where the baryon yields are smaller than meson yields. The baryonic contributions may broaden the width of the rho-meson

even more. But we argue that they will not qualitatively change the behavior of T_{eff} in the mass range considered in this paper, considering that the mesonic resonance contributions do not qualitatively change the dilepton spectra and then the behavior of T_{eff} compared to the dominant $\pi\pi$ process in this mass range. Note that Π_ρ^R depends on thermal distributions of mesons and then on local temperature $T(x)$ and medium velocity $u(x)$ determined by hydrodynamic simulation, which are functions of space-time position. We only take into account the processes mediated through the ρ meson, because the di-electron production is dominated by the isovector channel instead of the isoscalar one. According to the flavor $SU(3)$ quark model, the relative weight of the electromagnetic couplings for vector mesons $V = \rho, \omega, \phi$ is about 9:1:2, roughly consistent to the electromagnetic decay widths $\Gamma_{V \rightarrow ee} = 7.0, 0.6, 1.27$ KeV respectively [8]. On the other hand, ω and ϕ mesons can be easily identified in experiments. We also neglect the Dalitz decay channels for η and π^0 : $\eta \rightarrow e^+e^-\gamma$, $\mu^+\mu^-\gamma$ and $\pi^0 \rightarrow e^+e^-\gamma$. The pion spectrum is mainly below $m_\pi = 135$ MeV and irrelevant to our current range of M . The η contribution can be easily deducted as the background in experiments due to its very long lifetime (about 1.5×10^5 fm/c), leading to decays outside the freezeout scope.

After making approximation $n_B(p \cdot u) \approx e^{p \cdot u/T}$ and then integrating over the lepton pair rapidity y , we obtain the differential cross section for an expanding fireball [27],

$$\begin{aligned} \frac{d^4 N}{p_T dp_T M dM d\phi_p} &\approx -\frac{\alpha}{2\pi^4} \frac{1}{M^2} \left(1 + \frac{2m^2}{M^2}\right) \sqrt{1 - \frac{4m^2}{M^2}} \\ &\times \int d^4 x \exp \left[\frac{1}{T} \gamma_T M_T v_T p_T \cos(\phi_v - \phi_p) \right] K_0 \left(\frac{\gamma_T M_T}{T} \right) \text{Im}\Pi^R, \end{aligned} \quad (3)$$

where $p_T \equiv |\mathbf{p}_T|$ is the scalar transverse momentum of the lepton pair, ϕ_p and ϕ_v are the azimuthal angles of \mathbf{p}_T and the local transverse fluid velocity \mathbf{v}_T respectively, $\gamma_T = 1/\sqrt{1 - v_T^2}$ is the local transverse Lorentz factor for the fluid element, and K_0 is the modified Bessel function of the second kind. Note that the encoding of space-time history of the fireball is realized by integrals over fluid coordinates $d^4 x = \tau d\tau d\eta d^2 \mathbf{x}_T$, where τ, η are proper time and space-time rapidity respectively and \mathbf{x}_T is the transverse position of the fluid element. For central collisions with azimuthal symmetry, the angular integral can be worked out by $\int d\phi \exp[x \cos \phi] = 2\pi I_0(x)$ analytically with I_0 being the modified Bessel function of the first kind.

The evolution of the rate with the proper time τ is shown in the left panel of Fig. 2. The emission rate is proportional to $T^4 S \tau$ where S is the transverse area. For the harder EOS like the QGP ideal gas there is a rapid expansion leading to a very fast decreasing of T and S . As a result the QGP freezes out in a very short time with less dilepton emission. But with softer EOS like the lattice one, T decreases slowly as S expands, making the freezeout isothermal lines expand and remain almost constant at large radii, which greatly increases the di-electron emission in the HG phase.

The numerical results for the invariant mass spectra of the multiplicity with the LAT-EOS in central collisions are shown in the right panel of Fig. 2. The contributions from the QGP and the HG components are distinguished. The shapes of the spectra with the QGP-EOS only or the HG-EOS only are similar to the QGP or HG component (blue-dashed/red-dotted line) here. One can see that the QGP/HG contribution dominates in the region $M \gtrsim 1$ GeV. The emission from the QGP phase in the early stage with high temperatures contributes to the hard parts of the spectra with large M and m_T . The HG phase in later stage with low temperature contributes in small M region and is shaped by the ρ meson form factor, but a sizable collective flow developed in this stage can harden the transverse momentum spectra [27]. Also we have shown the HG contribution from the $\rho\pi\pi$ vertex only, which is lower than the full HG contribution (with all resonances below 1300 MeV included) in the lower mass region. This indicates the broadening effect to the ρ meson spectra from the resonances' contribution.

III. EFFECTIVE TEMPERATURE, ELLIPTIC FLOW AND M_T SCALING

To discuss the sensitivity of dilepton signals to different stages and collectivity developed in the history of the fireball, it is valuable to investigate dilepton transverse momentum spectra and its inverse slope parameter. We can use the reduced transverse mass $m_T \equiv M_T - M$ with $M_T = \sqrt{M^2 + p_T^2}$ to replace p_T as the variable. After carrying out the space-time integrals we assume that the transverse spectra can be approximately parameterized as [28, 29],

$$\frac{d^2 N}{m_T dm_T M dM} \sim \sqrt{\frac{T}{\gamma_T}} \frac{\sqrt{m_T + M}}{m_T} \exp \left(-\frac{m_T + M}{T_{eff}} \right), \quad (4)$$

FIG. 2: (Color online) Differential multiplicity as a function of proper time(left panel) and the di-electron invariant mass (right panel). The LAT-EOS [26] is used in the calculation and the contributions from the QGP and HG are shown in dashed and dotted lines, respectively. The dashed-dotted-dotted line is the HG contribution from the $\rho\pi\pi$ vertex only. The contribution from the HG is dominated by ρ mesons.

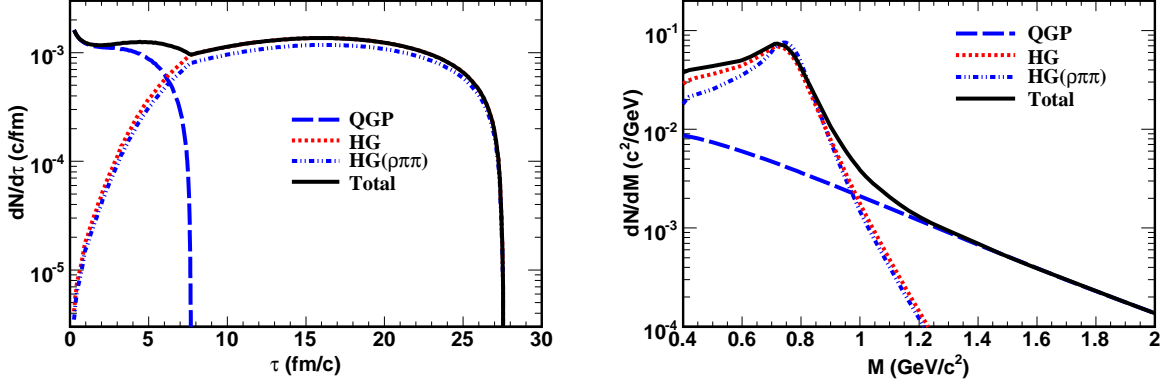
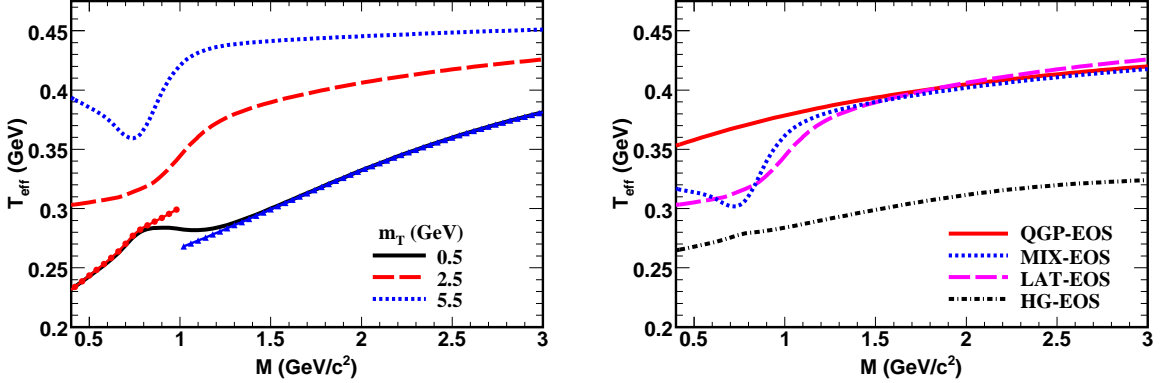


FIG. 3: (Color online) Left panel: slope parameter T_{eff} as a function of M with the LAT-EOS and for three m_T values. Results for three m_T values are shown as solid, dashed and dotted lines. For $m_T = 0.5$ GeV, thin red and blue lines with circles and triangles represent the results extracted from contributions of the HG and QGP phases, respectively. Right panel: The slope parameter T_{eff} calculated for four equations of state at fixed $m_T = 2.5$ GeV.



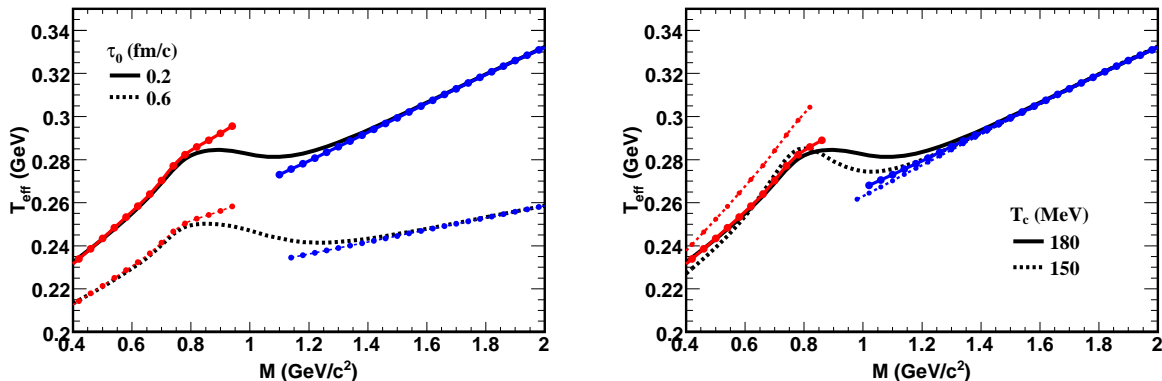
with the average temperature \bar{T} , the average transverse velocity \bar{v}_T of the fluid and its Lorentz factor $\bar{\gamma}_T = 1/\sqrt{1-\bar{v}_T^2}$. The asymptotic forms of the slope parameter T_{eff} can be written as,

$$T_{eff} \sim \begin{cases} \bar{T} + M^* \bar{v}_T^2, & \text{for } p_T \ll M \\ \bar{T} \sqrt{\frac{1+\bar{v}_T}{1-\bar{v}_T}}, & \text{for } p_T \gg M \end{cases}, \quad (5)$$

where M^* is a monotonic function of M . As emissions in different space-time are encoded in the spectra (4), the slope parameter T_{eff} depends on the fitting window of M and p_T , so do \bar{T} and \bar{v}_T .

The slope parameters T_{eff} versus M from the LAT-EOS are shown in the left panel of Fig. 3. For low p_T , e.g. $m_T = 0.5$ GeV, T_{eff} approximately follows $T_{eff} \sim \bar{T} + M^* \bar{v}_T^2$ as in Eq. (5). The curves below 1 GeV have smaller \bar{T} and larger \bar{v}_T , while above 1 GeV they have an opposite trend. For even higher M the increase of T_{eff} is not caused by the collective flow since larger M reflects the higher temperature in earlier emission when the collective flow has not fully developed. The disconnected curves with solid circles and triangles are T_{eff} extracted from the contributions of the HG or QGP phase only. They reflect different trends of T_{eff} below/above 1 GeV from the HG/QGP phase. When m_T is larger, e.g. $m_T = 2.5$ GeV, T_{eff} does not follow the above formula for low p_T , but the same trends still exist. For very large m_T , e.g. $m_T = 5.5$ GeV, T_{eff} follows the blue-shift formula $T_{eff} \sim T \sqrt{\frac{1+\bar{v}_T}{1-\bar{v}_T}}$, which is independent of M . The valley at $M \sim m_\rho$ is due to the fact that the QGP component (with higher T_{eff}) is dominant

FIG. 4: Slope parameter T_{eff} as a function of M with the dependence on the initial time τ_0 (left panel) and on the phase transition temperature T_c (right panel). We choose $m_T = 0.5$ GeV and use LAT-EOS for both panels. The red and blue lines with circles represent the results extracted from contributions of the HG and QGP phases, respectively.



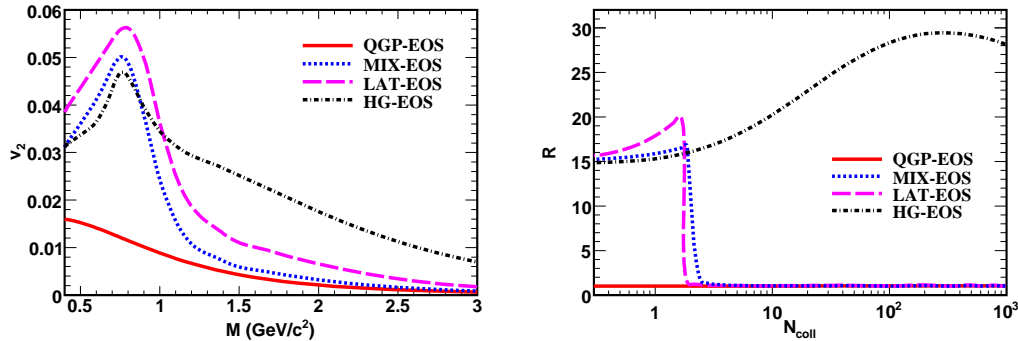
over the HG one (with lower T_{eff}) except in the region near $M \sim m_\rho$. One can see in the figure that T_{eff} increases with m_T , since the larger m_T probe the earlier state of the fireball with high temperatures. For the MIX-EOS, since there is a large contribution from the coexisting stage of two phases with the same temperature and fluid velocity, the difference in T_{eff} between the QGP and HG phases is smaller than the case of the LAT-EOS. For other two types of EOS, the QGP and HG ones, T_{eff} simply increase with M monotonously. In right panel of Fig. 3, we compare T_{eff} with different EOS. It is found that the magnitude of T_{eff} for the HG-EOS is much smaller than that for other EOS with partonic phase. Such behaviors of di-electron T_{eff} are expected to be measured and tested in the future experiments.

In Fig. 4 we show the dependence of T_{eff} on the initial time τ_0 for hydrodynamic evolution and the phase transition temperature T_c . When we tune τ_0 from 0.2 fm/c to 0.6 fm/c and change the initial peak temperature from 520 MeV to 350 MeV, or in other words, delay the hydrodynamic process, the magnitudes of T_{eff} , \bar{T} and \bar{v}_T decrease due to smaller initial temperature and acceleration but their structure remains the same. When changing T_c from 180 to 150 MeV, the magnitude of T_{eff} does not change much, but the slope increases in the small M region. This can be understood because a smaller transition temperature means that the HG phase occupies outer layer of the fireball with larger radial flow velocities.

Now we can compare our result for T_{eff} with NA60 data [21]. The T_{eff} curve of NA60 is extracted from low m_T spectra. It is comparable to our result in Fig. 4 with $m_T = 0.5$ GeV. But the trend above $M = 1$ GeV in NA60 data is different: it is downward while our curve is upward after a transition region between 0.8 and 1.2 GeV. We now give the reason for such a difference. We note that the region of $M > 1$ GeV probes earlier stage of the fireball, where the QGP emission dominates over the hadronic emission. Such a different trend is just the manifestation of the radial flow and average temperature effects of the QGP phase. At the NA60 energy, the life of the QGP phase (if there is any) is much shorter and its average temperature is lower (near freeze-out T_f), the radial flow does not have enough time to develop and the average temperature is just above T_f . For $M < 1$ GeV, the dominant contribution is from the hadronic phase which appears at later stage of the evolution and has larger collective flow, so T_{eff} is larger since it has a component proportional to the flow velocity squared times an effective mass, see first line of Eq. (5). That is the reason for the upward/downward trend below/above 1 GeV at the NA60 energy. In contrast, at the RHIC energy, the life of the QGP phase is longer and there is some time for the radial flow to develop and make T_{eff} larger. Another effect is that the average temperature in the QGP phase is larger than at the NA60 energy. This is the reason for the upward trend above 1 GeV in our result.

For non-central or peripheral collisions we can compute the elliptic flow coefficient v_2 versus transverse momentum and invariant mass, $v_2(p_T, M) = \langle \cos(2\phi_p) \rangle$. Setting the impact parameter $b = 7$ fm, we calculate dilepton v_2 as a function of invariant mass for four EOS, see the left panel of Fig. 5. The results with the MIX-EOS or LAT-EOS have similar features to Ref. [9]. Dilepton sources within different mass windows are sensitive to different stages of the expansion history. We see that v_2 is much smaller for larger M than that for smaller M . This is because dileptons at larger M come mainly from the QGP phase at earlier time of the fluid evolution with smaller collective flow, while those at smaller M are mainly from the HG phase at later stage when the collective flow is fully developed. The HG contribution is characterized by the peak at ρ meson mass which quantitatively different from the partonic contribution. If there is only one phase in the course of the evolution, these distinct feature will disappear. The initial temperature of the QGP phase in EOS containing the QGP phase is much higher than that of the pure HG

FIG. 5: Elliptic flow v_2 (left panel) and the ratio R for the M_T scaling (right panel) for different EOS. For v_2 the impact parameter is set to $b = 7$ fm. For R we scan all values of the impact parameter, i.e. $b = [0, 15]$ fm.



phase in HG-EOS at the same initial energy density. So the early stage emission from the former is much larger than that from the latter (since yield is proportional to T^4), then the later stage emission for HG-EOS has much larger proportion in the total yield. This helps us understand the bigger elliptic flow of HG-EOS than that of other EOS containing the QGP phase in the intermediate mass region. As the temperature window for emission with HG-EOS is not very wide and the low mass dileptons come mostly from the low temperature stage, similar to the surface emission of hadrons, the elliptic flow has a slight increase with mass in the low mass region. The peaks at the ρ meson mass in the MIX-EOS and LAT-EOS cases and the increase in the small mass region are partially caused by the surface emission, but the main reason is the influence of the QGP phase in the region below the ρ meson mass [9].

We also note that if the QGP is created, the dilepton spectrum in the mass region between the ϕ meson mass and J/ψ mass depends approximately only on its transverse mass M_T . This can be seen from Eq. (3), after the integration over azimuthal angle ϕ_p , the differential yield is proportional to $I_0(\gamma_T v_T p_T/T) K_0(\gamma_T M_T/T)$. In the continuum region, the lepton mass, the quark mass and the collectivity are negligible, then the yield is only a function of M_T . This property is called the M_T scaling [30]. It can be broken when transverse expansion becomes appreciable or hadronic gas emission with extra mass scales dominate the yield. By looking at the ratio,

$$R = \frac{dN/dM_T^2 dp_T^2 dy|_{M_T=2.6\text{GeV}, p_T=2\text{GeV}}}{dN/dM_T^2 dp_T^2 dy|_{M_T=2.6\text{GeV}, p_T=0\text{GeV}}}, \quad (6)$$

we study the M_T scaling with more realistic hydrodynamic evolution. As shown in the right panel of Fig. 5, the scaling is rather robust if the QGP phase is present. We find that the elliptic expansion, the collective flow of the QGP and the ρ meson form factor do not qualitatively change the result in Ref. [30], if the di-electron yields from partonic/hadronic source dominate in the intermediate/low mass region respectively.

IV. SUMMARY AND CONCLUSION

In conclusion, we have investigated the thermal production of di-electrons in the quark-gluon plasma created in heavy ion collisions at RHIC energy. Different types of the equations of state are used in our study. The phase transition from hadron gas to quark-gluon plasma leads to a rich structure for the thermal dilepton production. The mass dependence of the inverse slope parameter is sensitive to the collective dynamics of the medium: at the mass region ($M \lesssim 1$ GeV), it is dominated by the hadronic interactions while in the intermediate mass region ($1 \lesssim M \lesssim 3$ GeV), partonic interactions become important. At lower transverse momenta, the slope parameter for mixed-phase and lattice EOS shows different trends in M in the low mass region (hadronic phase) and intermediate mass regions (partonic phase), which reflects the existence of two distinct phases. In this case, there is transition area around $M = 1$ GeV to connect two T_{eff} components with different trends. In the hadronic phase in the lower mass region the flow velocity is found to be stronger than that in the partonic phase in the higher mass region. Around $M \sim 1$ GeV, the slope parameter is found sensitive to the equation of state of the fireball used in our calculation. The elliptic flow and the M_T scaling are calculated which show distinct features for the hadronic and partonic phases. We have investigated the surface emission or the emission in a fixed interval of temperatures, where we have found that these features are absent for the two phases. In this sense the dilepton emission is a volume effect which can carry the information of the space-time history of the fireball. Therefore all these features of the collective flow can serve as clean probes to hot and dense medium created in high energy heavy ion collisions.

Acknowledgement: JD and QW thank Hao-jie Xu for his help in adding the mesonic resonance contribution. QW is supported in part by the '100 talents' project of Chinese Academy of Sciences (CAS) and by the National Natural Science Foundation of China (NSFC) with grant No. 10735040. NX is supported in part by the Department of Energy (DOE) with grant No. DE-AC03-76SF00098. PZ is supported in part by the National Natural Science Foundation of China (NSFC) with grant Nos. 10847001 and 10975084. JD is supported by China Postdoctoral Science Foundation with grant No. 20080440722.

-
- [1] L. D. McLerran and T. Toimela, Phys. Rev. D **31**, 545 (1985).
 - [2] K. Kajantie, J. I. Kapusta, L. D. McLerran and A. Mekjian, Phys. Rev. D **34**, 2746 (1986).
 - [3] R. Rapp, G. Chanfray and J. Wambach, Phys. Rev. Lett. **76**, 368 (1996) [arXiv:hep-ph/9508353].
 - [4] R. Rapp, G. Chanfray and J. Wambach, Nucl. Phys. A **617**, 472 (1997) [arXiv:hep-ph/9702210].
 - [5] R. Rapp and C. Gale, Phys. Rev. C **60**, 024903 (1999) [arXiv:hep-ph/9902268].
 - [6] R. Rapp and J. Wambach, Adv. Nucl. Phys. **25**, 1 (2000).
 - [7] J. Alam, S. Sarkar, P. Roy, T. Hatsuda and B. Sinha, Annals Phys. **286**, 159 (2001).
 - [8] H. van Hees and R. Rapp, Nucl. Phys. A **806**, 339 (2008).
 - [9] R. Chatterjee, D. K. Srivastava, U. W. Heinz and C. Gale, Phys. Rev. C **75**, 054909 (2007).
 - [10] K. Dusling and S. Lin, Nucl. Phys. A **809**, 246 (2008).
 - [11] P. Mohanty, J. e. Alam and B. Mohanty, arXiv:1008.1112 [nucl-th].
 - [12] R. D. Pisarski, Phys. Lett. B **110**, 155 (1982).
 - [13] R. Arnaldi *et al.* [NA60 Collaboration], Phys. Rev. Lett. **96**, 162302 (2006).
 - [14] H. van Hees and R. Rapp, Phys. Rev. Lett. **97**, 102301 (2006).
 - [15] J. Ruppert, C. Gale, T. Renk, P. Lichard and J. I. Kapusta, Phys. Rev. Lett. **100**, 162301 (2008).
 - [16] A. Adare *et al.* [PHENIX Collaboration], Phys. Lett. B **670**, 313 (2009).
 - [17] K. H. Ackermann *et al.* [STAR Collaboration], Phys. Rev. Lett. **86**, 402 (2001).
 - [18] K. Adcox *et al.* [PHENIX Collaboration], Phys. Rev. Lett. **89**, 212301 (2002).
 - [19] M. Gyulassy, L. McLerran, Nucl. Phys. A **750**, 30(2005).
 - [20] E. V. Shuryak, Nucl. Phys. A **750**, 64 (2005).
 - [21] R. Arnaldi *et al.* [NA60 Collaboration], Phys. Rev. Lett. **100**, 022302 (2008).
 - [22] T. Renk and J. Ruppert, Phys. Rev. C **77**, 024907 (2008).
 - [23] P. F. Kolb, J. Sollfrank and U. W. Heinz, Phys. Rev. C **62**, 054909 (2000).
 - [24] D. Teaney, J. Lauret and E. V. Shuryak, Phys. Rev. Lett. **86**, 4783 (2001).
 - [25] J. Sollfrank, P. Huovinen, M. Kataja, P. V. Ruuskanen, M. Prakash and R. Venugopalan, Phys. Rev. C **55**, 392 (1997).
 - [26] A. Bazavov *et al.*, arXiv:0903.4379 [hep-lat].
 - [27] K. Kajantie, M. Kataja, L. D. McLerran and P. V. Ruuskanen, Phys. Rev. D **34**, 811 (1986).
 - [28] E. Schnedermann, J. Sollfrank and U. W. Heinz, Phys. Rev. C **48**, 2462 (1993).
 - [29] M. I. Gorenstein, K. A. Bugaev and M. Gazdzicki, Phys. Rev. Lett. **88**, 132301 (2002).
 - [30] M. Asakawa, C. M. Ko and P. Levai, Phys. Rev. Lett. **70**, 398 (1993).